

Chapter 5

Optical Studies

Photoluminescence Analysis

5.1 Luminescence

It is the phenomenon in which electronic states of solid are excited by some energy sources (Infrared, ultraviolet, visible light for PL and heating in TL) and excitation energy is re-emitted as a light of longer wavelength (Stokes Law). Light is directed onto a sample, where it is absorbed and imparts excess energy into the material in a process called photo-excitation. One way this excess energy can be dissipated by the sample is through the emission of light, or *luminescence*. In the case of photo-excitation, this luminescence is called *photoluminescence*. Photo-excitation causes electrons within a material to move into permissible excited states. When these electrons return to their equilibrium states, the excess energy is released and may include the emission of light (a radiative process) or may not (a non-radiative process). The energy of the emitted light (photoluminescence) relates to the difference in energy levels between the two electron states involved in the transition between the excited state and the equilibrium state. The quantity of the emitted light is related to the relative contribution of the radiative process. Photoluminescence spectroscopy is a contactless, non-destructive method of probing the electronic structure of materials.

The optical properties of PbWO_4 nanomaterial are different than that of the bulk material. It is observed that with decrease in size optical absorption band shifts to the blue side. This is ascribed to the quantum size effect which can well explained by electron in a box model. Due to their spatial confinement the kinetic energy of electron increases. This results in a broadening of band gap.

5.2 General characteristics of Photoluminescence spectra of PbWO_4

The emission spectra of scheelite tungstates AWO_4 ($A = \text{Pb, Cd, Ba, Ca, etc.}$) exhibit always broad luminescence band in the blue spectral region. PbWO_4 at room temperature exhibits ABO_4 crystal structure with tetragonal unit cell with A^{2+} (Pb^{2+}) as cation and a tetrahedral BO_4^{2-} (WO_4^{2-}) as anion. The tetrahedrons consist of a W^{6+} ion at the center, surrounded by four O^{2-} ions. It is well known that the luminescence spectrum of PWO is composed of two main bands; the “blue” one peaking around 420 nm and the “green” one peaking between 490 and 540 nm. There are two defects: 1. a regular lattice (WO_4)⁻² defect and 2. a defect based WO_3 center, which are responsible for the complex character of PbWO_4 emission. The blue luminescence is an intrinsic feature of PWO, and is generally ascribed to the radiative decay of a self-trapped exciton that locates on the regular WO_4 group [1]. The green luminescence is of extrinsic origin and it was ascribed to a defect based WO_3 center [2] possibly with F center [3]. The concentration of these defects are strongly influenced by the raw material and the method used for the crystal growth.

5.3 Electronic Structure of PbWO_4

According to the band theory given by C.Zheng et al., the bottom of conduction band (CB) is formed by both 5d state of W^{6+} ion and 6p state of Pb^{2+} ion in PbWO_4 , and the coping of valence band (VB) is formed by both 6s state of the Pb^{2+} ion and 2p state of O^{2-} ion, as shown in Figure 5.1.

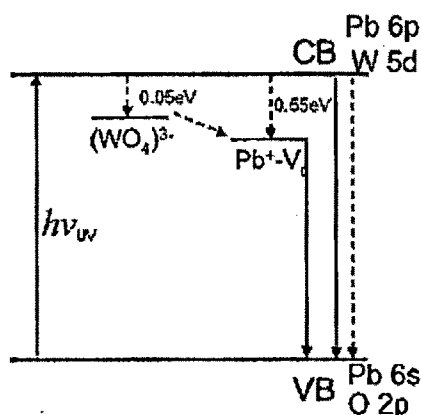


Figure 5.1 Band Structure of PbWO_4

The $\text{W}5d$ states are degenerated and split in a crystal field of tetragonal symmetry in e and t_2 vibrational modes. The $\text{Pb } 6s$ state and $\text{Pb } 6p$ state have appreciable contributions throughout the valence band and conduction band, respectively. The valence-band width is calculated to be 5.5 eV. The $\text{Pb } 6s$ state forms a narrow band 1 eV below the bottom of the valence band.

When the PbWO_4 is excited within fundamental absorption band, charge transfer by two types of electronic transitions can be observed,

- (i) From O^{2-} to W^{6+} within WO_4^{2-} oxyanion complex
- (ii) From O^{2-} to Pb^{2+} outside WO_4^{2-} oxyanion complex

5.4 Self Trapped Exciton (STE)

An electron from oxygen 2p goes into one of the empty tungsten 5d orbital (the bottom of W5d) in the WO_4^{2-} group by absorbing ultraviolet irradiation in PbWO_4 . In the excited state of the WO_4^{2-} group, the hole (on the oxygen) and the electron (on the tungsten) remain together as an exciton because of their strong interactions. This type of exciton which is produced in PbWO_4 is called Frenkel exciton. The exciton binding energy was estimated as being about 0.1 eV. The lowest exciton transition is connected to an electronic excitation from the mixed $\text{Pb}(6s) \rightarrow \text{O}(2p)$ ground states to the mixed $\text{Pb}(6p) \rightarrow \text{W}(5d)$ excited states. As the Pb contributions to the top of the valence band and the bottom of the conduction band are small in raspite compared to scheelite so the exciton transition in raspite is very weak. That is to say, the raspite exciton is a molecular-type exciton of the WO_6 -anion complex with mainly covalent bonding within the oxo-complex. The electronic band structures of both phases are, as a whole, similar to each other except exciton transition.

5.5 Crystal-field splitting and hybridization of the molecular orbital of WO_4^{2-} tetrahedral group

In Figure 5.2, the schematic diagram of a crystal field splitting and hybridization of the molecular orbitals of an oxyanion tetrahedral complex is shown.

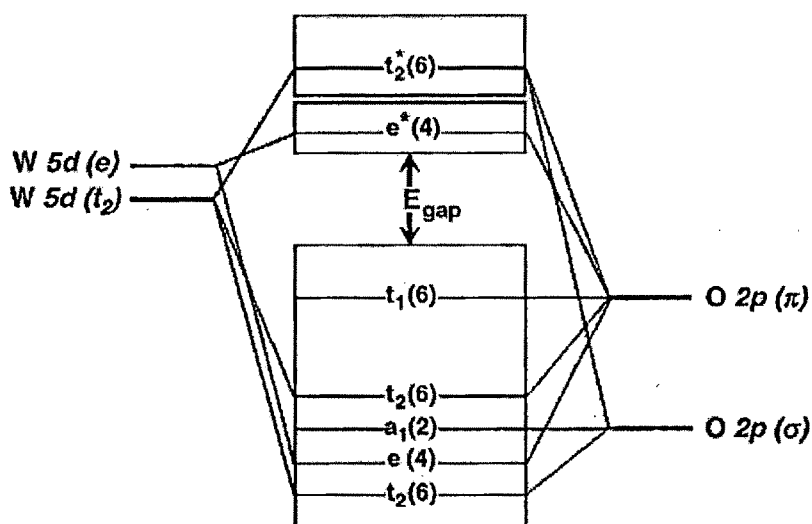


Figure 5.2 schematic diagram of a crystal field splitting and hybridization WO_4^{2-} group [4].

The crystal-field splitting and hybridization of the molecular orbitals of WO_4^{2-} tetrahedral are shown in Figure 5.2. The $\text{W}5d(t_2)$ and $\text{W}5d(e)$ orbitals are hybridized with the $\text{O}2p(\sigma)$ and $\text{O}2p(\pi)$ ligand orbitals to form WO_4^{2-} tetrahedra. The four ligand $2p(\sigma)$ orbitals are compatible with the tetrahedral representation for a_1 and t_2 symmetries and the eight ligand $2p(\pi)$ orbitals are for t_1 , t_2 and e symmetries. The top occupied state has t_1 symmetry formed from $\text{O}2p(\pi)$ states. The lowest unoccupied state has e symmetry formed from a combination of the $\text{W}5d(e)$ and $\text{O}2p(\pi)$ orbitals to give antibonding (*). The hybridization between the $\text{W}5d$ and $\text{O}2p$ orbitals is specified as covalent bonding between the ions. For ground state

system, all one-electron states below band gap are filled to give a many electron 1A_1 state. At the lowest excited state, there is one hole in t_1 (primarily O $2p(\pi)$) state and one electron in e (primarily W5d) state which give rise to many-electron 1T_1 , 3T_1 , 1T_2 and 3T_2 states. Among them, only $^1T_2 \rightarrow ^1A_1$ transition is electric dipole allow [4, 5]. However, due to the inducement of Jahn–Teller effect [6] and electron–phonon interactions [7], the WO_4^{2-} complex in many tungstate crystals was slightly distorted from T_d to D_{2d} symmetry so that the inhibited transitions of WO_4^{2-} complex, such as 1T_2 , 1T_1 , 3T_2 and 3T_1 to 1A_1 , became partially allowable.

5.6 Cerium

The rare earth (RE) ions most commonly used for applications as phosphors, lasers, and amplifiers are the so-called lanthanide ions. The ground state of all the Lanthanide atoms is probably either $[\text{Xe}] 4f^n 5d^1 6s^2$ or $[\text{Xe}] 4f^{n+1} 6s^2$, where the increase in n from 0 to 14 corresponds to the change from La ($Z=57$) through to Lu ($Z=71$). Rare earth ions have unfilled optically active 4f electrons screened by outer electronic filled shells. Because of these unfilled shells, these kinds of ions are usually called *paramagnetic ions*.

Cerium is the most abundant member of the series of elements known as lanthanides or rare earths. Cerium is the second and most reactive member of the lanthanides series. Cerium is characterized chemically by having two stable valence states one is Ce^{4+} , *ceric*, and the other is Ce^{3+} , *cerous*. The cerium atom ($Z=58$), which has an outer electronic configuration $[\text{Xe}]4f^1$ i.e. $5s^2 5p^6 5d^1 4f^1 6s^2$. It is very electro-positive and has predominantly ionic chemistry due to the low ionization potential for the removal of the three most weakly bound electrons. These atoms are usually incorporated in crystals as trivalent cations i.e. Ce^{3+} .

In trivalent ions 5d, 6s, and some 4f electrons are removed and so $(\text{RE})^{3+}$ ions deal with transitions between electronic energy sublevels of the $4f^n$ electronic configuration. The $4f^n$ electrons are, in fact, the valence electrons that are responsible for the optical transitions. These valence electrons are shielded by the 5s and 5p outer electrons of the $5s^2 5p^6$ less energetic configurations. Because of this shielding effect, the valence electrons of Ce^{3+} ion are weakly affected by the ligand ions in PbWO_4 crystals; a situation results the case of a weak crystalline field. For Weak crystalline field: $H_{\text{CF}} \leq H_{\text{SO}}, H_{\text{ce}}, H_{\text{O}}$. Consequently, the spin-orbit interaction term of the free Ce^{3+} ion Hamiltonian is dominant over the crystalline field Hamiltonian term. In this case, the energy levels of the free Ce^{3+} ion are only slightly perturbed (shifted and split) by the crystalline field. This causes the $^{2S+1}L_J$ states of the $(\text{RE})^{3+}$

ions to be slightly perturbed when these ions are incorporated in crystals. The effect of the crystal field is to produce a slight shift in the energy of these states and to cause additional level splitting. However, the amount of this shift and the splitting energy are much smaller than the spin-orbit splitting, and thus, the optical spectra of $(RE)^{3+}$ ions are fairly similar to those expected for free ions. The free ion wavefunction are then used as basis functions to apply perturbation theory, H_{CF} being the perturbation Hamiltonian over the $^{2S+1}L_J$ states (where S and L are the spin and orbital angular momenta and $J = L + S$). This approach is generally applied to describe the energy levels of trivalent rare earth ions, since for these ions the 4f valence electrons are screened by the outer $5s^2 5p^6$ electrons. These electrons partially shield the crystalline field created by the B ions).

5.7 Luminescence of PbWO₄ due to Scheelite phase

5.7.1 Blue emission

The lowest exciton of PWO is mainly characterized by $6s^2 \rightarrow 6s6p$ cationic transitions in Pb²⁺ ions. It is thus believed that the excitons or electron-hole pairs generated optically on Pb²⁺ ions move to the regular WO₄²⁻ groups, to emit the blue Luminescence [8].

Scheelite phase of PbWO₄ gives rise to the luminescence blue band at 2.80 eV (440nm) when excitation energy is in exciton band region (4 to 5 eV) (250-300nm). This luminescence has been regarded as being an intrinsic feature of Scheelite phase of PbWO₄. The 2.80-eV luminescence is ascribed to the radiative decay of self-trapped (localized) excitons in regular WO₄²⁻ group. J. A. Groenink and G. Blasse [9] conclude that the blue emission with maximum at 420 nm, is due to transitions in the regular tungsten [WO₄²⁻] group in which the Pb²⁺ play a role.

5.7.2 Green emission

The origin of green emission of PbWO₄ was reported in many papers. However the defects responsible for the origin of green emission are controversial and still under discussion.

5.7.3 Two Green emission bands G(I) and G(II)

The presence of two green emission bands at Room Temperature was reported [10-13].

5.7.4 G(I) emission band

The G(I) emission band, observed at low temperatures, located around 2.3–2.4 eV (510-530 nm) and excited around 3.9 eV (310 nm) in undoped crystals is assumed to arise from the [WO₄²⁻] groups located in the crystal regions of lead-deficient structure.

5.7.5 G(II) emission band

The G(II) emission band, observed at high temperatures ($T > 160\text{K}$) located at 2.5 eV (495 nm) appears under excitation around 4.07 eV (310nm) observed due to isolated oxygen vacancies in irregular WO_3 groups also called F-centers [14-19]. Green emission was also connected with raspite inclusions produce due to thermal stress during crystal growth process [20-22]. The green emission was ascribed to the MoO_4^{2-} anion groups which is a stable electron trap [23-27]. It was suggested that Mo^{6+} ions are present not only in the Mo^{6+} -doped crystals but also in undoped crystals. The molybdenum ion is chemically very similar to the tungsten ion it is difficult to separate in the course of raw material preparation. The molybdenum impurity is usually present in PbWO_4 at the level of < 1 ppm. The presence in the lead-deficient PbWO_4 crystals of the superstructure of the type of $\text{Pb}_{7.5}\text{W}_8\text{O}_{32}$ was reported in Ref.[28]. In Ref. [29], this superstructure was assumed to be responsible for the green emission. In Refs.[30], the green emission was connected with defects of the type of $\{\text{WO}_4 + \text{O}_i\}$. According to C.Shi. green luminescence is not produced by $(\text{WO}_3 + \text{F})$ centers lacking oxygen but probably arises from $(\text{WO}_4 + \text{O}_i)$ centers (O_i - Oxygen interstice) with an excess local oxygen.

5.8 Effect of Lead Source on PhotoLuminescence of PbWO₄ Phosphor

Sun et al. [31] showed that PL emission of SrWO₄ can be modified by the morphology. According to him different morphologies contribute to the formation of different surface defects that influence in the PL behaviour.

SEM and TEM analysis of undoped as well as Cerium doped PbWO₄ reveals that different Lead sources produce various morphologies of PbWO₄ as shown in below Table 5.1.

Table 5.1 Summary of Phase produced, Morphologies and Particle size of undoped and Cerium doped PbWO₄ prepared using different Lead sources.

Lead Source	Dopant	Phase	Morphology	Dimension
Pb(CH ₃ COO) ₂	-	stolzite	dendrite	1 μm
		stolzite	tetrahedron	500nm
Pb(CH ₃ COO) ₂	CeO ₂	raspite	flat nanobelt	5 μm x 1 μm
		stolzite	octahedron microparticles	1.5 μm
Pb(NO ₃) ₂	-	raspite	flat nanobelt	5 μm x 1 μm
		stolzite	six branched dendrites	2 μm
		stolzite	rhombic particles	500nm
Pb(NO ₃) ₂	CeO ₂	stolzite	tetrahedron	100nm
PbCl ₂	-	raspite	micro plates	few μm
		stolzite	micro particles	100nm
PbCl ₂	CeO ₂	stolzite	tetrahedron	100nm

5.8.1 Lead Acetate and Lead Nitrate as Lead Sources

The effect of different lead sources [$\text{Pb}(\text{CH}_3\text{COO})_2$, $\text{Pb}(\text{NO}_3)_2$ and PbCl_2] on the formation of PbWO_4 and $\text{PbWO}_4:\text{Ce}$ were investigated from Photoluminescence characterization. Photoluminescence property of undoped and Cerium doped PbWO_4 prepared with different Lead sources at 100°C is studied and discussed below.

As discussed in the previous chapters, when $\text{Pb}(\text{CH}_3\text{COO})_2$ was used as the lead source, product with mixture of two phases (stolzite and raspite) were produced. Dendrite and tetrahedron type morphology is produced due to stolzite phase. On doping with Cerium, flat nanobelt due to raspite phase and Octahedron shaped microparticles due to stolzite phase are obtained. Figure 5.3(a) represents the PL spectra of as synthesised products. When $\text{Pb}(\text{NO}_3)_2$ was used as the lead source, six branched dendrite and rhombic shaped particles of PbWO_4 are produced due to stolzite phase and flat nanobelt are produced due to raspite phase. Doping of Cerium in PbWO_4 produces tetrahedron shaped particles due to stolzite phase. PL spectra of as synthesised products are shown in Figure 5.3(b). When PbCl_2 used as lead source, microparticles of PbWO_4 are produced due to stolzite phase and flat microbelts are produced due to raspite phase. When Cerium was doped in PbWO_4 , tetrahedron shaped particles with stolzite phase were produced. Figure 5.3(c) represents the PL spectra of as synthesised products. In general, two phases (stolzite and raspite) are produced in all the samples irrespective of Lead sources and both the phase produces have different morphologies of PbWO_4 phosphor in micrometer range.

First we will discuss our published result [32] of PL spectra of undoped and cerium-doped PbWO_4 by using lead acetate and lead nitrate as a lead source. The PL spectra of undoped and cerium-doped PbWO_4 by using lead chloride as a lead source will be discussed later separately.

The PL spectra of undoped and cerium-doped PbWO_4 were investigated at room temperature using a 305-nm excitation wavelength. Comparison of PL spectra of two lead sources (Lead Acetate and Lead Nitrate) is shown in Figure 5.3(a). The effect of Cerium doping on PL spectra of PbWO_4 prepared by using lead acetate and lead nitrate is shown in Figure 5.3(b) and Figure 5.3(c), respectively.

Literature survey reveals that the emission spectra of PbWO_4 consists of two components, a fast blue component around 450 nm which is an intrinsic feature of scheelite phase and a slow green one around 480–520 nm which is an intrinsic feature of rhabdophane phase. The broad blue–green emission band around 450–550 nm is observed in all four samples which is in good agreement with reported values [33]. A broad blue luminescence peak around 450 nm is observed in all samples which originate from tetragonal WO_4^{2-} groups [34]. The origin of such complex spectra is already discussed in the beginning of this chapter. Effect of different morphologies on Photoluminescence emission of PbWO_4 and cerium doped PbWO_4 is the main motive of this part of our experiment.

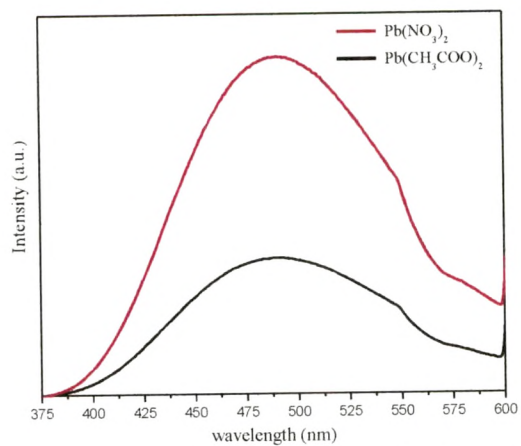


Figure 5.3(a) PL spectra of PbWO_4 synthesized with different Lead Sources

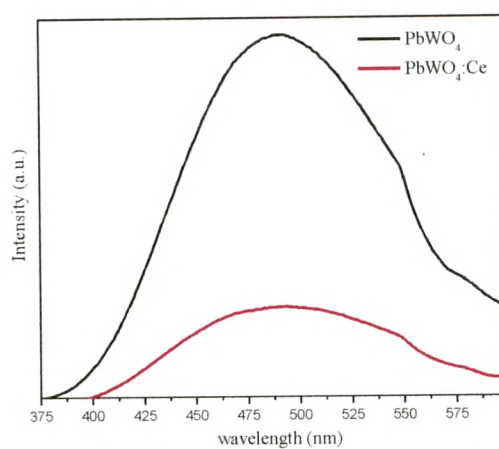


Figure 5.3(b) PL spectra of PbWO_4 synthesized with Lead Acetate

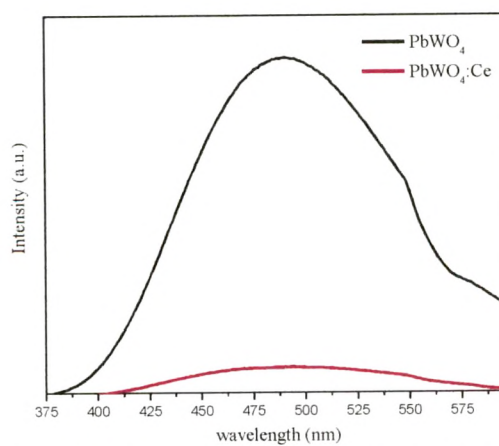


Figure 5.3(c) PL spectra of PbWO_4 synthesized with Lead Nitrate

Comparison of Photoluminescence spectra of PbWO_4 microcrystallites clearly shows the variation in PL intensity. The PL intensity is higher for PbWO_4 prepared with lead nitrate and low for PbWO_4 prepared with lead acetate as shown in Figure 5.3(a). PbWO_4 prepared with lead nitrate has mixed morphologies (six branched dendrite + rhombic nanoparticles + nanobelt) and PbWO_4 prepared with lead acetate also possesses mixed morphologies (single branched dendrite + tetrahedron microparticles). The dendrite with six branched structure has highest surface to volume ratio among all the morphologies produced here [35]. Rhombic shaped nanoparticles and nanobelt also have higher surface area compared to single branched dendrite and tetrahedron microparticles. Higher the surface to volume ratio means higher concentration of surface related defects (particularly oxygen vacancies) and hence high light collection efficiency. These characteristics enhance PL emission in PbWO_4 prepared with lead nitrate compared to PbWO_4 prepared with lead acetate.

The intensity of PL is suppressed to a great extent by doping with cerium which is shown in Figure 5.3(b) and Figure 5.3(c). The cerium doped PbWO_4 shows weaker luminescence intensity than that of undoped PbWO_4 . Ce^{3+} ($4f^1$) is the most simple rare earth ion with one electron case having excited configuration $5d^1$. As discussed earlier in Ce^{3+} spin orbit interaction is dominant over crystal field interaction, hence energy levels of Ce^{3+} ion are not perturbed by PbWO_4 crystal field. The $4f^1$ ground state configuration yields two levels: $^2F_{5/2}$ and $^2F_{7/2}$ due to spin orbit coupling and the $5d^1$ configuration is split by the crystal field in 2 to 5 components between the band gap of PbWO_4 . The emission occurs from the lowest crystal field component of the $5d^1$ configuration to the two levels of the ground state. Since the $5d \rightarrow 4f$ transitions are parity allowed and spin selection is not appropriate, the emission transitions is a fully allowed one. The reduction in PL intensity is due to these nonradiative $5d \rightarrow 4f$ transition in the cerium doped PbWO_4 . Therefore Ce^{3+} ions could serve as efficient non-radiative traps in PbWO_4 crystal lattice [36].

The green emission of undoped crystals was ascribed to the WO_3 oxygen-deficient complex anion in scheelite phase [37]. This emission was connected with the inclusions of the raspite structure formed due to the thermal stress appearing in the process of crystal growth [38]. PL intensity of $\text{PbWO}_4:\text{Ce}$ prepared with lead acetate is more compared to $\text{PbWO}_4:\text{Ce}$ prepared with lead nitrate. Structural investigation of Cerium doped samples shows that $\text{PbWO}_4:\text{Ce}$ prepared with lead acetate contains more inclusions of raspite phase as compared to $\text{PbWO}_4:\text{Ce}$ prepared with lead nitrate.

5.8.2 Lead Chloride as a Lead Source

According to our literature survey no one has prepared PbWO_4 by using Lead chloride as a lead source except Changhua An et al. [39]. In his paper he compared the PL spectra of PbWO_4 prepared with two different lead sources, Lead Nitrate and Lead Chloride. He found that the PL emission of PbWO_4 prepared with Lead Chloride has highest intensity compared to PbWO_4 prepared with Lead Nitrate. Enhancement of PL intensity due to Lead Chloride as a lead source to synthesis PbWO_4 encourage us to do further investigation reported in this thesis.

Figure 5.4 shows room temperature PL emission spectra of PbWO_4 and Cerium doped PbWO_4 prepared using PbCl_2 as lead source with excitation wavelength 254 nm. PL spectra of PbWO_4 samples prepared with PbCl_2 are somewhat different than that prepared with Lead acetate and Lead nitrate.

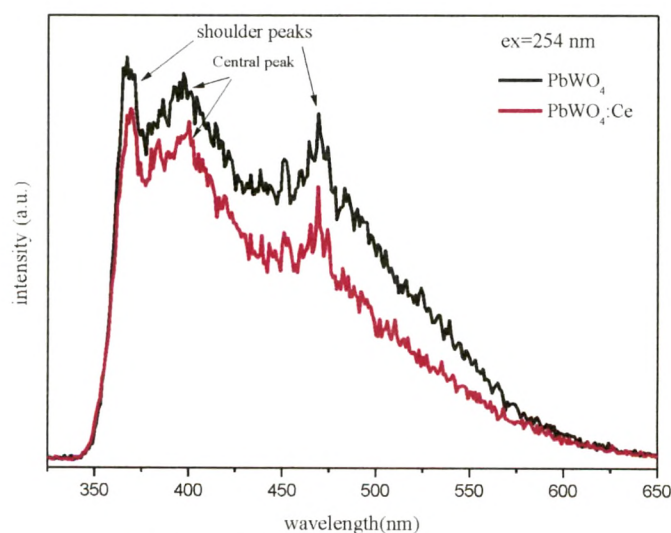


Figure 2. PL spectra of PbWO_4 prepared with Lead Chloride

Figure 5.4 PL spectra of PbWO_4 prepared with Lead Chloride at 100°C

As expected both samples show broad blue-green emission in visible region. The PL spectra has “*spread-eagle-shape*” with a central peak surrounded by two broad shoulder peaks. Emission spectrum reveals that it is composed of several sub-bands which are almost distributed throughout entire 350-550 nm region.

According to morphological studies of these samples shows that when PbCl_2 used as lead source, microparticles of PbWO_4 are produced due to stolzite phase and flat microbelts are produced due to raspite phase. When Cerium doped in PbWO_4 , tetrahedron shaped particles with stolzite phase were produced. The decomposition of PL spectra into individual Gaussian components results four Gaussians to achieve a good agreement with the experimental data. In order to do detailed analysis of luminescence spectra it is fitted with four individual Gaussian components shown in Figure 5.4(a) and Figure 5.4(b) and named Gaussian peak I, II, III and IV respectively. Variation in locations and intensity of strongly overlapped Gaussian components of photoluminescence spectra of PbWO_4 and $\text{PbWO}_4:\text{Ce}$ prepared at 100°C is shown in Table 5.2 and discussed here.

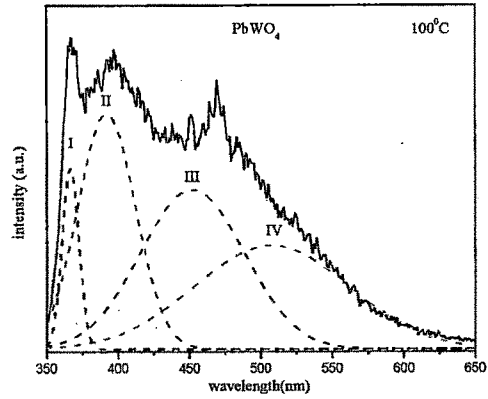


Figure 5.4(a)

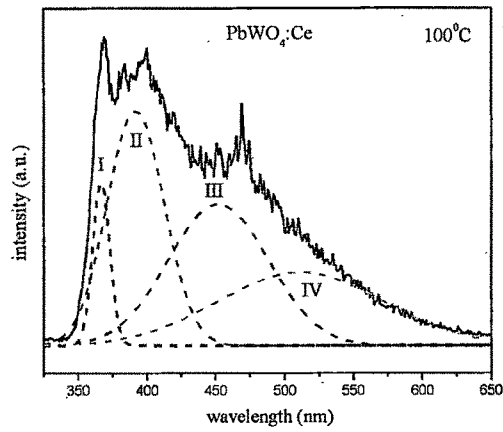


Figure 5.4(b)

Table 5.2 The locations and Intensity of Gaussian components of PL spectra of PbWO_4 and $\text{PbWO}_4:\text{Ce}$ prepared at 100°C .

Temp. 100°C	Gaussian peak I		Gaussian peak II		Gaussian peak III		Gaussian peak IV	
	wavelength (nm)	intensity (a.u.)	wavelength (nm)	intensity (a.u.)	wavelength (nm)	intensity (a.u.)	wavelength (nm)	intensity (a.u.)
PWO	367	40	392	52	452	35	507	23
PWO:Ce	367	32	392	45	452	27	512	14

Photoluminescence emission spectra shows structured character for both undoped and cerium doped samples. Such type of structural shape invokes presence of four Gaussian components: three peaks fall in blue region and one in green region. The presence of four Gaussian components indicates the excited states of emission center are relaxed and degenerated under the influence by some type of perturbation.

It is already discussed that blue emission is attributed to the radiative recombination of STE localized in regular WO_4^{2-} complex of scheelite phase. Isolated WO_4^{2-} complex has tetrahedral symmetry T_d with ground state configuration $(t_1)^6(e)^0$ [41,42]. Excited configuration $(t_1)^5(e)^1$ results four electronic states: two singlets and two triplets: ${}^1T_2 < {}^1T_1 < {}^3T_2 \cong {}^3T_1$ [43]. It is accepted that blue luminescence originates from the ${}^3T_2 \cong {}^3T_1 \rightarrow {}^1A_1$ [44]. Because of the symmetry lowering from T_d to C_{3v} due to the JT effect, the 3T_1 state splits into the 3A_2 and 3E sublevels, and the 3T_2 state into the 3A_1 and 3E sublevels [45]. The schematic diagram is shown in Figure 5.5.

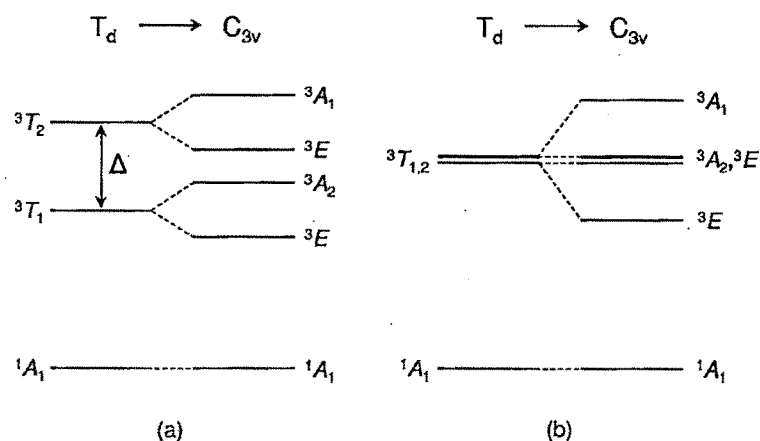


Figure 5.5 Splitting of Triplet states due to Jahn-Teller effect [45]

Here we proposed that the Gaussian peak I (367 nm), the Gaussian peak II (392 nm) and the Gaussian peak III (452 nm) may correspond to the radiative transitions from ${}^3A_1 \rightarrow {}^1A_1$, ${}^3A_2 \cong {}^3E \rightarrow {}^1A_1$ and ${}^3A_2 \rightarrow {}^1A_1$, respectively. Hence blue emission occurs from the lower lying triplet state split by Jahn-Teller interaction.

The peak position of all the three blue Gaussian components in PL spectra recorded at room temperature is shifted towards the short wavelength side compared to those reported at lower temperatures. This type of blue shift is also reported by M.Itoh which can be explained well by configurational coordinate diagram. Similar blue shift has also been observed in CdWO_4 [46] and CaWO_4 [47]. The G(II) band which is dominant at lower temperatures also do major contribution at room temperature.

The Gaussian peak IV (around 510 nm) corresponds to green emission which is assumed to arise from oxygen deficient regular WO_3 group also called F center. Oxygen vacancies V_O (or F^{++}) can capture one or two electrons from $[\text{WO}_4^{2-}]$ to form F^+ or F centers and so $[\text{WO}_4^{2-}]$ is changed into WO_3 . This crystal defect (lack of oxygen) is related to surface in scheelite phase. This emission as a result of the photo-thermally stimulated disintegration of localized exciton states and subsequent recombination of the produced electron and hole centres near WO_3 groups. As our sample also contains raspite phase, this emission also ascribed to intrinsic luminescence probably originates from localized exciton in octahedral WO_6^{6-} groups in the raspite phase. Raspite-type inclusions which exist in our samples usually crystallize in a scheelite-type structure. The transformation from raspite to scheelite is expected to take place by thermal stress because of the very small volume difference between the two forms. These inclusions probably result from the thermal stress that is unavoidably introduced in PbWO_4 crystals.

The intensity of four individual Gaussian peaks of Cerium doped PbWO_4 microcrystallites reduce to different extents compared with that of pure PbWO_4 samples. According to Kobayashi et al. Cerium doping in PbWO_4 results low energy shift of absorption spectra due to $4f \rightarrow 5d$ transitions and hence emission spectra should also shift to lower energy side due to Stokes shift. Similar type of red shift is observed in position of Gaussian peak IV in our case. Furthermore, decrease of light yield (LY) for PWO:Ce sample by a factor 2–3 was observed with respect to undoped PWO. The absence of intrinsic Ce^{3+} emission at the room temperature and observed lower Light Yield can be explained by a non-radiative $5d \rightarrow 4f$ transition to the ground state of excited Ce^{3+} ions, i.e. Ce^{3+} ions can serve as efficient non-radiative traps in the PWO matrix. Such a conclusion support the observed faster PL decay of PWO: Ce at room temperature (RT) with respect to the undoped sample, which can be explained by selective suppression of the delayed recombination process due to non-radiative recombination of free electrons and holes at the Ce^{3+} sites.

PL spectra of all the PbWO_4 microcrystallites prepared with different lead sources having different morphologies shows very weak size-dependency indicate that the sizes of these structures are so big that they are beyond the border of the quantum confinement regime.

5.9 Effect of Synthesis Parameters on Photoluminescence

As discussed in the previous chapters regarding structural studies, different reaction parameters produced different types of crystal structures and morphologies as shown in below Table 5.3.

Table 5.3 Summary of reaction conditions, phase, morphologies and particle size of undoped and Cerium doped PbWO_4 prepared using different Lead chloride.

Sample	PbCl_2 conc. (M)	Na_2WO_4 conc. (M)	Ce conc. (M)	Temp. (°C)	Time (h)	pH	Morphology	Average particle size (nm)
5	0.01	0.01	-	100	4	7	micro plates	few μm
							micro particles	100nm
6	0.01	0.01	0.001	100	4	7	tetrahedron	100nm
8	0.01	0.01	-	125	4	7	spherical nanoparticles	20-40 nm
							Hollow nano tubes	12.37 nm (OD) 80-170 nm (L)
9	0.01	0.01	-	125	4	11	nanorods	40nm (OD) 2 μm (L)
13	0.1	0.1	0.001	200	12	7	spherical nanoparticles	50-100 nm

5.10 Excitation Spectra

Figure 5.6 represent the excitation spectra of undoped PbWO_4 . This excitation spectra was collected for a Sample No 8. The excitation spectrum for 400 nm emission has a wide broad band peaking at 250 nm , and a weaker band at 296 nm and a second weaker new band is observed at 615 nm. Excitation spectra of remaining samples also shows similar behavior which are not shown.

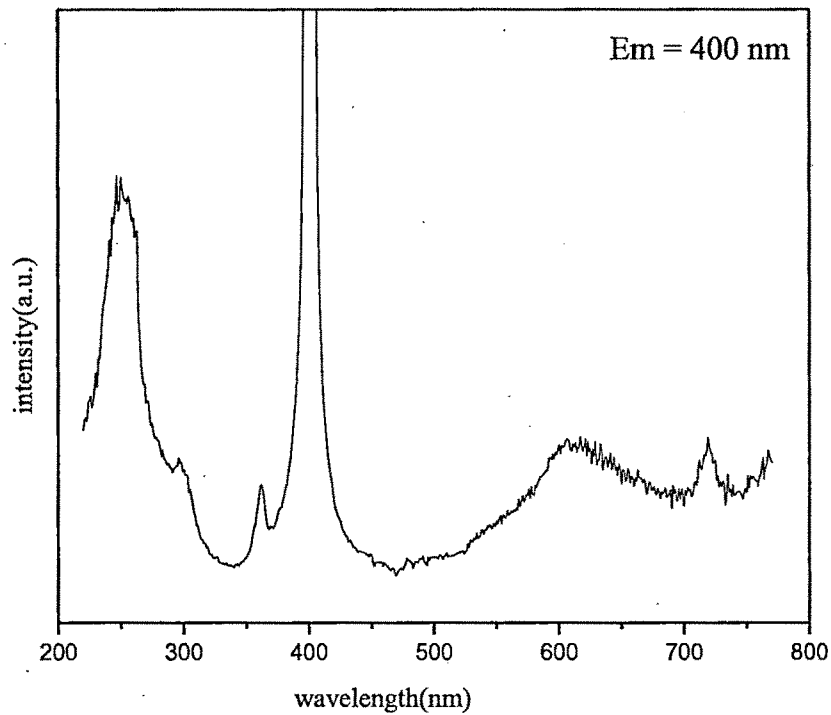


Figure 5.6 Excitation spectra of PbWO_4 (sample 8)

5.11 Emission Spectra

Figure 5.7 shows combined emission spectra of undoped and cerium doped PbWO_4 phosphors. This spectra reveals that different reaction parameters have great influence on the photoluminescence which is discussed upcoming sections. Below Table shows summary of the different reaction conditions kept during experiment.

PbWO_4 prepared at different reaction conditions

Sample No.	PbCl_2 conc. (M)	Na_2WO_4 conc. (M)	Ce conc. (M)	Temp. ($^{\circ}\text{C}$)	Time (h)	pH
5	0.01	0.01	-	100	10	7
6	0.01	0.01	0.001	100	10	7
7	0.01	0.01	-	125	10	3
8	0.01	0.01	-	125	10	7
9	0.01	0.01	-	125	10	11
10	0.01	0.01	-	150	10	7
11	0.01	0.01	0.001	150	10	7
12	0.01	0.01	-	200	10	7
13	0.01	0.01	0.001	200	10	7
14	0.01	0.01	0.001	R.T.	10	7

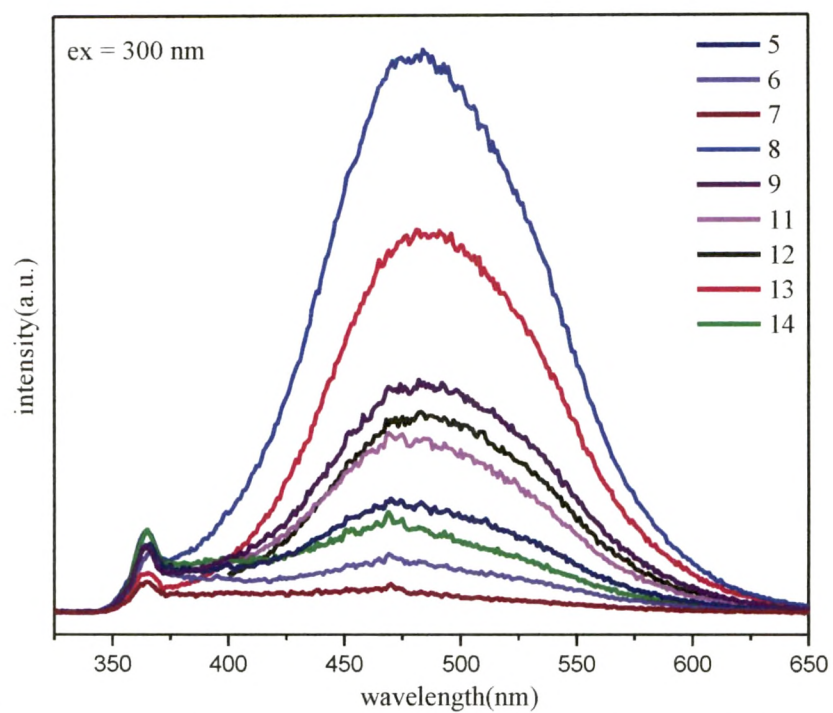


Figure 5.7 Effect of Synthesis parameters on PhotoLuminescence intensity

5.12 PL spectra of undoped and Cerium doped PbWO_4 synthesized at 200°C

Figure 5.8 shows room temperature photoluminescence spectra of undoped and Cerium doped PbWO_4 nanophosphor synthesized 200°C at excited with 254 nm wavelength. As expected both the samples show broad “spread-eagle-shaped” blue-green with integral luminescence intensity of emission falls in 350-600 visible region.

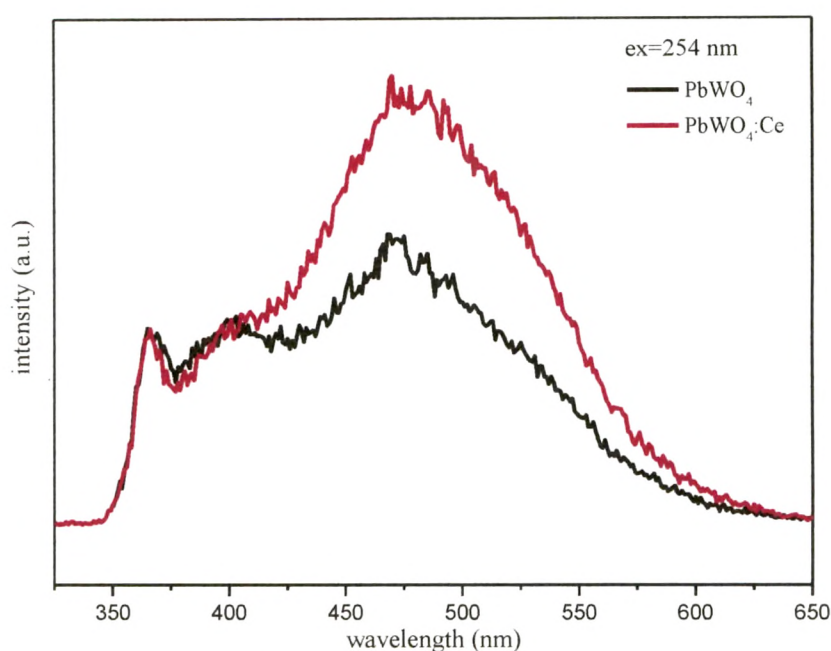


Figure 5.8 PL spectra of PbWO_4 synthesized at 200°C

The decomposition of PL spectra into individual Gaussian components results four Gaussians to achieve a good agreement with the experimental data shown in Figure 5.8 (a) and (b). In order to do detailed analysis of luminescence spectra it is fitted with four individual Gaussian components and named Gaussian peak I, II, III and IV respectively. Variation in locations and intensity of strongly overlapped Gaussian components of photoluminescence spectra of PbWO_4 and $\text{PbWO}_4:\text{Ce}$ prepared at 200°C is shown in Table 5.4 and discussed here.

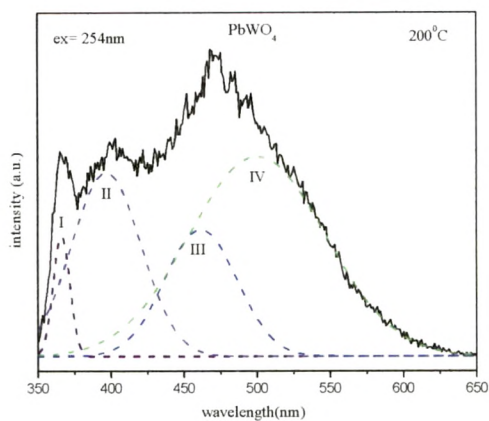


Figure 5.8 (a)

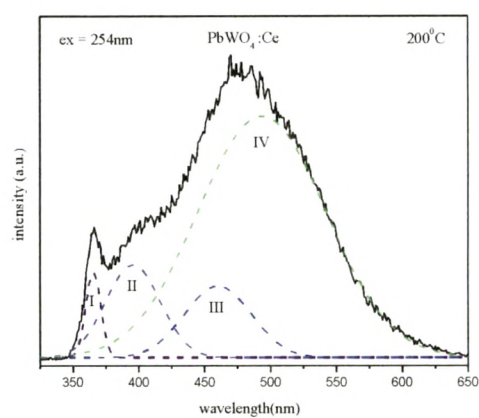


Figure 5.8 (b)

Table 5.4 The locations and intensity of Gaussian components of PL spectra of PbWO_4 and $\text{PbWO}_4:\text{Ce}$ prepared at 200°C .

Temp. ($^\circ\text{C}$)	Gaussian peak I		Gaussian peak II		Gaussian peak III		Gaussian peak IV	
	wavelength (nm)	intensity (a. u.)						
PWO	366	25	397	36	461	26	500	39
PWO:Ce	366	27	397	29	461	23	494	71

As already mentioned earlier the Gaussian peak I is observed at 366 nm, the Gaussian peak II at 397 nm and the Gaussian peak III at 461 nm may correspond to the radiative transitions from ${}^3A_1 \rightarrow {}^1A_1$, ${}^3A_2 \cong {}^3E \rightarrow {}^1A_1$ and ${}^3A_2 \rightarrow {}^1A_1$, respectively from the lower lying triplet state split by Jahn-Teller interaction in the regular WO_4^{2-} complex.

As shown in Figure 5.8(a) intensity of blue component B(II) is comparable to green component G(IV) in undoped $PbWO_4$. When $PbWO_4$ is doped with cerium intensity of blue components is suppressed and green luminescence is remarkably increases as shown in Table 5.4. The contribution of green emission Gaussian component G(IV) in Cerium doped $PbWO_4$ increase from 50% to 75% of the total light yield. Annealing at a temperature below 700°C suppressed the blue luminescence and enhanced its green components [48]. As both the samples prepared at 200°C contains only stolzite phase, possibility of enhancement of G(IV) component due to presence of raspite inclusions is ruled out. The only possible reason due to which green luminescence is increase is the higher synthesis temperature. In hydrothermal synthesis crystal growth occurs in close vessel called autoclave in the absence of sufficient air atmosphere. TEM images of Ce doped $PbWO_4$ synthesized at 200°C temperatures shows that they are spherical nanoparticles having size about 50-100 nm. At 200°C temperature during crystal growth of $PbWO_4:Ce$ oxygen near the surface of spherical nanoparticles get sufficient energy to escape from regular lattice site and creates (*Vo*) oxygen vacancies. At such high temperature oxygen escape from regular WO_4^{2-} complex and convert it to oxygen deficient WO_3 complex. Higher concentration of oxygen deficient WO_3 complex increase green luminescence. Thus decrease in concentration of WO_4^{2-} centers responsible for blue emission and increase in concentration of WO_3 centers responsible for green emission increases the contribution of green emission from 50% to 75%.

However, as reported previously, the green emission of $PbWO_4$ crystals is slower than the blue one in the decay characteristics [49]. Higher synthesise temperature can

enhance the green luminescence and give some contributions to the “slow” decay components which may be negative to the scintillating properties of PWO. Hence we conclude that Cerium doped PbWO_4 prepared at 200°C is not preferable to use for scintillation detector purpose.

5.13 Effect of pH on Photoluminescence of PbWO₄ nanophosphor

Structural (XRD and TEM) studies of undoped as well as Cerium doped PbWO₄ phosphor synthesized at different pH shows that the pH of the reaction solution plays an important role and it varies the crystallinity and morphology of the product considerably. In order to study the effect of pH of the reaction solution on luminescence property of PbWO₄ synthesized at different (3,7 and 11) pH, photoluminescence spectra of undoped PbWO₄ synthesized at different pH was recorded at two excitation wavelength 300 nm and 254 nm and are shown in Figure 5.9 and Figure 5.10, respectively.

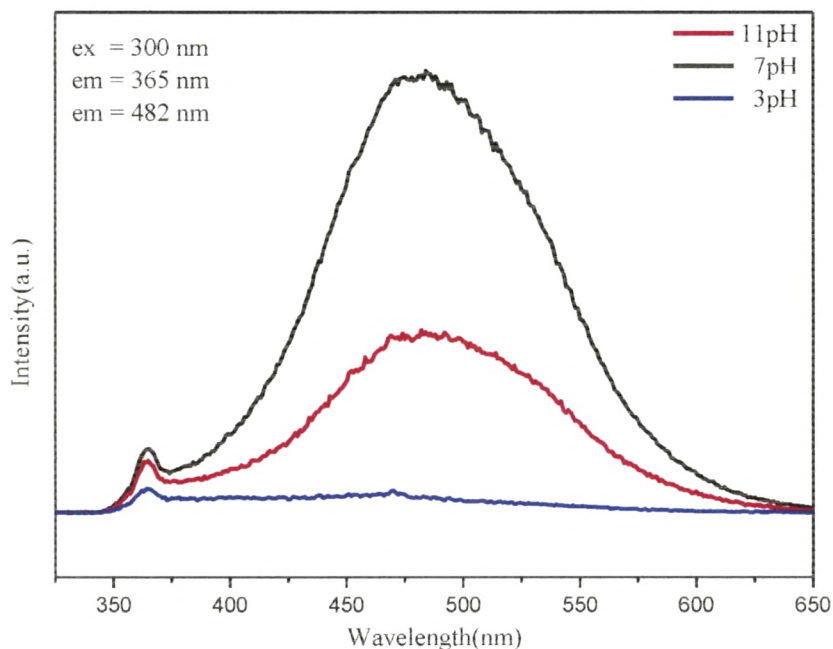


Figure 5.9 PL emission of PbWO₄ synthesized at different pH excited with 300nm

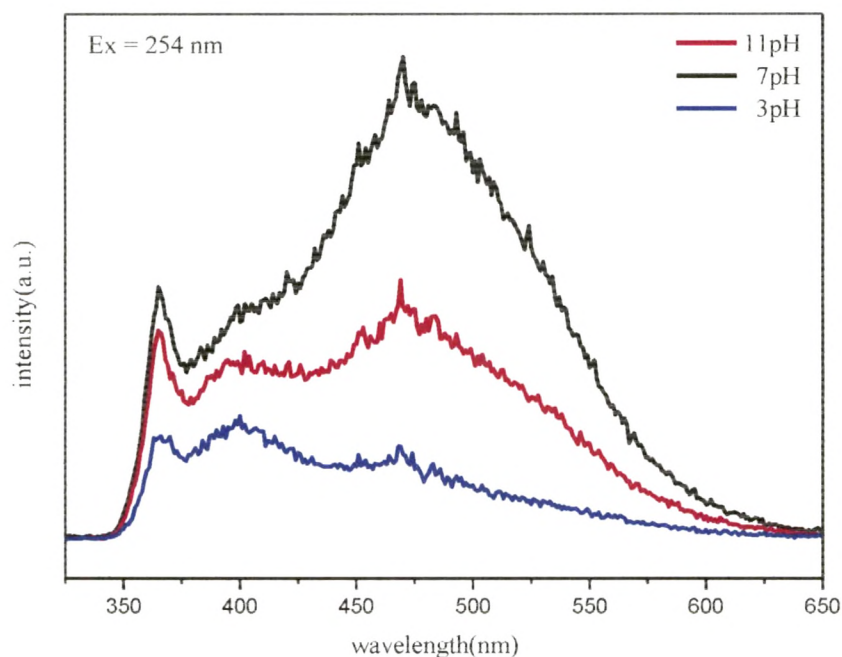


Figure 5.10 PL emission of PbWO₄ synthesized at different pH excited with 254 nm

Figure 5.10 shows room temperature photoluminescence spectra of nanocrystalline PbWO₄ powders prepared at three different (3, 7 and 11) pH of reaction solution excited with 254 nm wavelength. PbWO₄ shows “spread-eagle-shaped” broad luminescent emissions in blue and green range. As we can see from the PL spectra within the range of pH 3-11, the position of the emission peaks of the product remained almost unchanged for all the samples. In order to further obtain the detailed parameters about the luminescence properties of PbWO₄ microcrystals, we had fitted the emission spectra using four individual Gaussian lines to achieve good agreement with the experimental data which are shown below in Figure 5.10 (a-c). Variation in the location of Gausssian peaks and in their intensity is shown in Table 5.5.

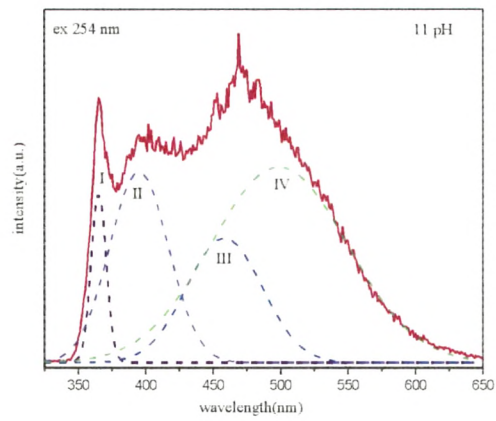


Figure 5.10(a)

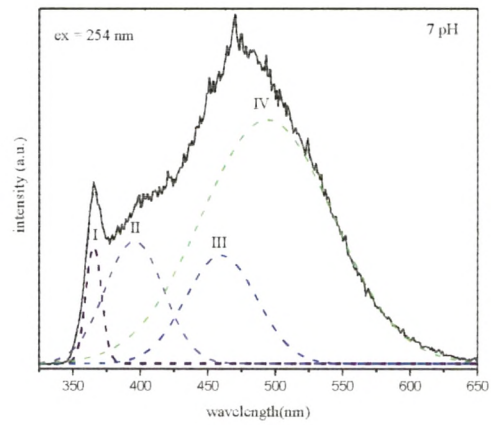


Figure 5.10(b)

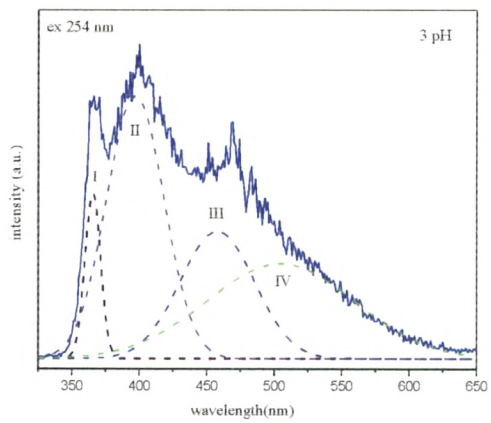


Figure 5.10(c)

Table 5.5 The locations and intensity of Gaussian components of PL spectra of PbWO₄ samples prepared at different pH

pH	Gaussian peak I		Gaussian peak II		Gaussian peak III		Gaussian peak IV	
	wavelength (nm)	intensity (a.u.)	wavelength (nm)	intensity (a.u.)	wavelength (nm)	intensity (a.u.)	wavelength (nm)	intensity (a.u.)
3	365	20	397	30	458	15	505	12
7	365	48	396	50	460	44	494	97
11	365	39	395	44	458	29	499	45

Obtained PL spectra was fitted with four individual Gaussian peaks having peaks position for peak I (365 nm), peak II (395 nm), peak III(459 nm) and peak IV (500nm) . Here we proposed that the Gaussian peak I, the Gaussian peak II and the Gaussian peak III may correspond to the radiative transitions from $^3A_1 \rightarrow ^1A_1$, $^3A_2 \cong ^3E \rightarrow ^1A_1$ and $^3A_2 \rightarrow ^1A_1$, respectively. Hence blue emission occurs from the lower lying triplet state split by Jahn-Teller interaction. The Gaussian peak IV ascribed to oxygen deficient irregular WO₃ neutral molecule.

According to XRD data, sample prepared with 7pH has highest crystallinity and sample prepared with 3pH has lowest crystallinity. Further increase in pH of the solution (7 to 11) crystallinity again reduced. It indicates that PL spectra of nano-sized PbWO₄ crystallites are strongly relied on their particle size and crystallinity. PL intensity has direct relation with crystallinity. The better crystallinity, the higher PL emission peak is.

PbWO₄ (Nanoparticles and HNTs) obtained at 7pH, display a strong emission peak centered at about 485 nm at room temperature. However, the absolute luminescence intensity increased with increasing pH, over the range of 3-7 pH, implying that the Nanoparticles and HNTs had much improved luminescence intensity. The very weak PL intensity of the sample obtained for pH 3 due to poor crystallinity.

The PL intensity of blue emission peak is highest for sample prepared at 7pH (HNTs), it is intermediate for sample prepared at 11pH (Nanorods) and lowest for sample prepared at 3pH which indicates that PbWO_4 HNTs have more regular lattice structure and uniform morphology compared to Nanorods. Sample prepared at 3pH has lowest regular lattice structure.

Similarly, The PL intensity of green emission peak is highest for sample prepared at 7pH (HNTs) intermediate for sample prepared at 11pH (Nanorods) and lowest for sample prepared at 3pH which indicates that PbWO_4 HNTs have highest defect centres relative to oxygen due to faster 1-D crystal growth compared to Nanorods and sample prepared at 3pH has lowest defect centres relative to oxygen.

Very high size-dependent emission of photoluminescence observed among these three products with different morphologies indicates that the sizes of these structures are so in the quantum confinement regime.

5.14 Effect of Synthesis Temperature on Photoluminescence of PbWO_4

Room Temperature Photoluminescence spectra of undoped PbWO_4 prepared at different temperatures is investigated and it is shown in Figure 5.11 for the 300nm excitation wavelength. The light-emitting property of the lead tungstate crystal is greatly influenced by synthesis temperature. PL spectra of all the samples exhibit emission in blue-green region with same emission peak position at 482 nm.

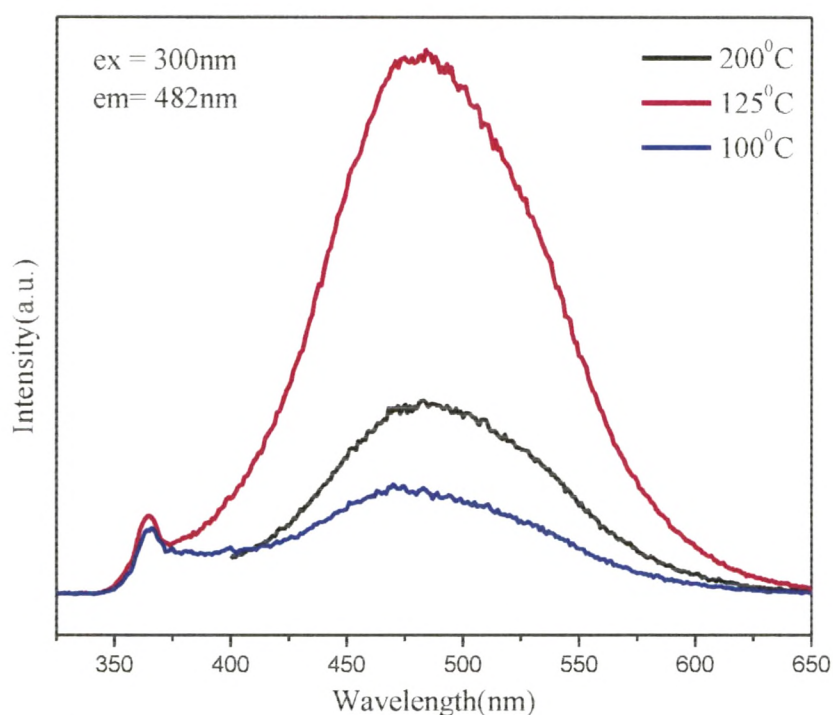


Figure 5.11 PL spectra of PbWO_4 synthesized at different temperatures

As we can see from the PL spectra, PL intensity is least for the sample prepared at 100 °C which increases for the sample prepared at 125 °C. PL intensity is again decrease for the sample prepared at 200°C. Apparently, raising the reaction temperature of the hydrothermal process would increase the luminescent intensity up to certain limits and further rise of

temperature lower the PL intensity. From this result, we can conclude that 125°C is the optimum temperature for the good intensity.

According to structural studies of these samples, PbWO₄ obtained at 100 °C are mixture of microparticles (100nm) with stolzite phase and micro plates (few μm) with raspite inclusions which have low crystallinity. Spherical nanoparticles (20-40 nm) and Hollow Nano Tubes (80-170 nm) of PbWO₄ having pure stolzite phase are obtained at 125 °C and they have highest crystallinity. XRD study of PbWO₄ sample prepared at 200°C shows that it has intermediate crystallinity between 125°C and 100°C.

It is well known that PL intensity has direct relation with crystallinity. The better crystallinity, the higher PL emission peak is. Morphologies and sizes also influence the luminescence properties of inorganic materials. Hence among all three samples (HNTs) of PbWO₄ prepared at 125 °C shows strong green luminescence due to its highest crystallinity while (microparticle + microplates) of PbWO₄ prepared at 100 °C shows weak luminescence due to poor crystallinity.

As already discussed higher crystallinity of Quasi-spherical nanoparticles and Hollow Nano Tubes are main reason to produce high PL intensity compared to low crystalline microparticles and flake like inclusions. It implied that PbWO₄ nanostructure have a better luminescence intensity then microstructure at room temperature.

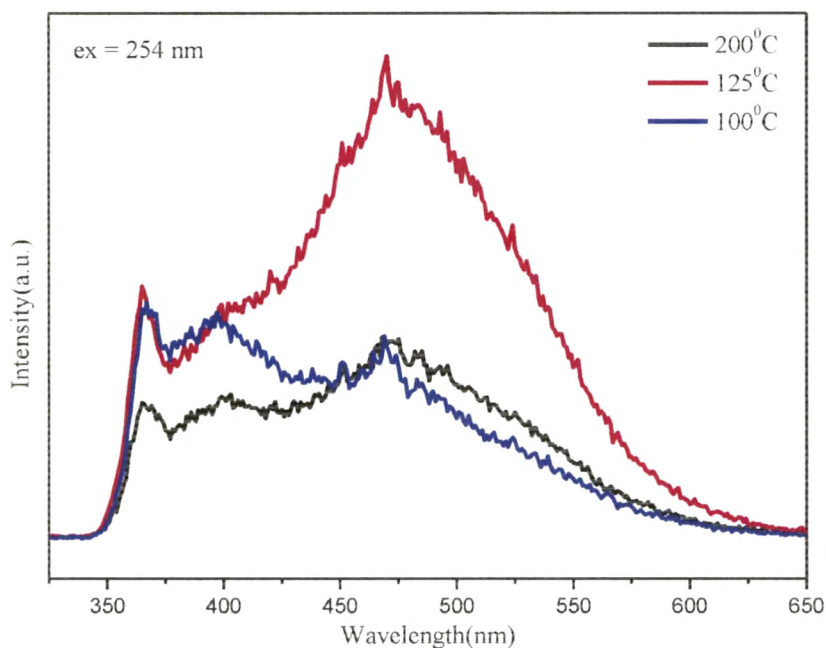


Figure 5.12 PL spectra of PbWO₄ prepared at different temperatures excited with 254nm

Figure 5.12 shows Room temperature photoluminescence spectra of PbWO₄ phosphor prepared at different temperatures excited with 254 nm wavelength. PbWO₄ shows broad luminescent emissions in blue and green range. In order to further obtain the detailed parameters about the luminescence properties of PbWO₄, we had decomposed the emission spectra using four individual Gaussian components to achieve good agreement with the experimental data which are shown in Figure 5.12 (a-c). Variation in the location of Gaussian peaks and in their intensity is shown in Table 5.6.

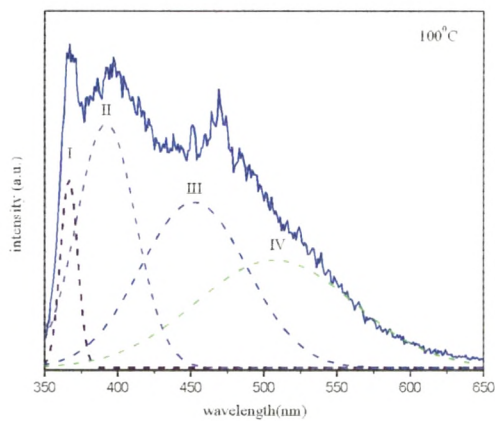


Figure 5.12(a)

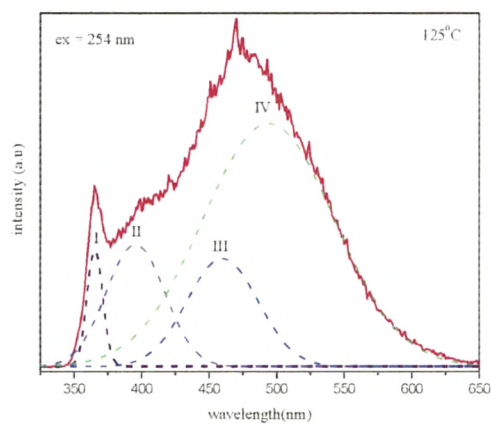


Figure 5.12(b)

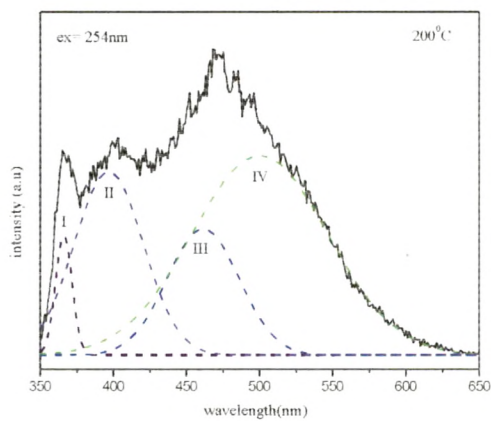


Figure 5.12(c)

Table 5.6 The locations and Intensity of Gaussian components of PL spectra of PbWO₄ samples prepared at different temperatures.

Temp. (°C)	Gaussian peak I		Gaussian peak II		Gaussian peak III		Gaussian peak IV	
	wavelength (nm)	intensity (a.u.)	wavelength (nm)	intensity (a.u.)	wavelength (nm)	intensity (a.u.)	wavelength (nm)	intensity (a.u.)
100	367	40	392	52	452	35	507	23
125	365	48	396	50	460	44	494	97
200	366	25	397	36	461	26	500	39

As we can see from the Table 5.6 positions of B(I) remain almost constant with temperature. The position of B(II) and B(III) components shift to lower energy side and the position of G(IV) component shift towards higher energy side first and then towards lower energy side. As already mentioned earlier the Gaussian peak I is observed around 365 nm, the Gaussian peak II at 396 nm and the Gaussian peak III at 460 nm may correspond to the radiative transitions from $^3A_1 \rightarrow ^1A_1$, $^3A_2 \cong ^3E \rightarrow ^1A_1$ and $^3A_2 \rightarrow ^1A_1$, respectively from the lower lying triplet state split by Jahn-Teller interaction in the regular WO_4^{2-} complex. The Gaussian peak IV corresponds to oxygen deficient WO_3 irregular complex in scheelite phase.

PbWO₄ microcrystallites prepared at 100°C contains mixed phase and microcrystals and microplates like morphologies. PbWO₄ prepared at 125°C has hollow nano tubes with pure stolzite phase structure while that prepared at 200°C has unknown morphology and pure stolzite phase confirmed from xrd spectra. Luminescence spectra of individual case are already discussed. Intensity of blue components B(I), B(II) and B(III) is higher at low temperatures and low at higher temperature. As we know that regular lattice group WO_4^{2-} is responsible for blue emission, higher intensity of blue emission at low temperature shows that samples prepared at low temperature has higher concentration of WO_4^{2-} . At higher reaction temperature lattice regularity breaks and also decrease the

concentration of blue emission center. Enhancement of Green emission of the sample prepared at 125°C is due to presence of larger amount of surface defect is also discussed.

5.15 Effect of Synthesis Temperature on Photoluminescence of $\text{PbWO}_4:\text{Ce}$

Similar to PL study of undoped PbWO_4 prepared at different temperatures, PL spectra of Cerium doped PbWO_4 prepared at different temperatures also investigated and it is shown in Figure 5.13 and Figure 5.14.

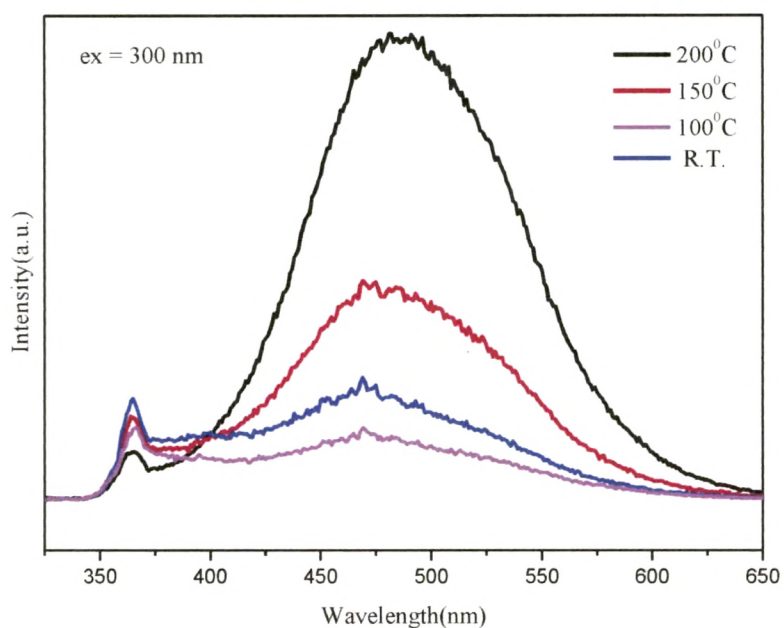


Figure 5.13 PL spectra of $\text{PbWO}_4:\text{Ce}$ prepared at different temperatures excited with 300nm. The light-emitting property of the Cerium doped lead tungstate crystal is greatly influenced by synthesis temperature. PL spectra of all the samples exhibit emission in blue-green region. Peak position of PL emission at room temperature is similar to that of undoped samples i.e. 482 nm but peak position is shifted to higher energy side for the samples prepared at higher temperatures i.e. 470 nm.

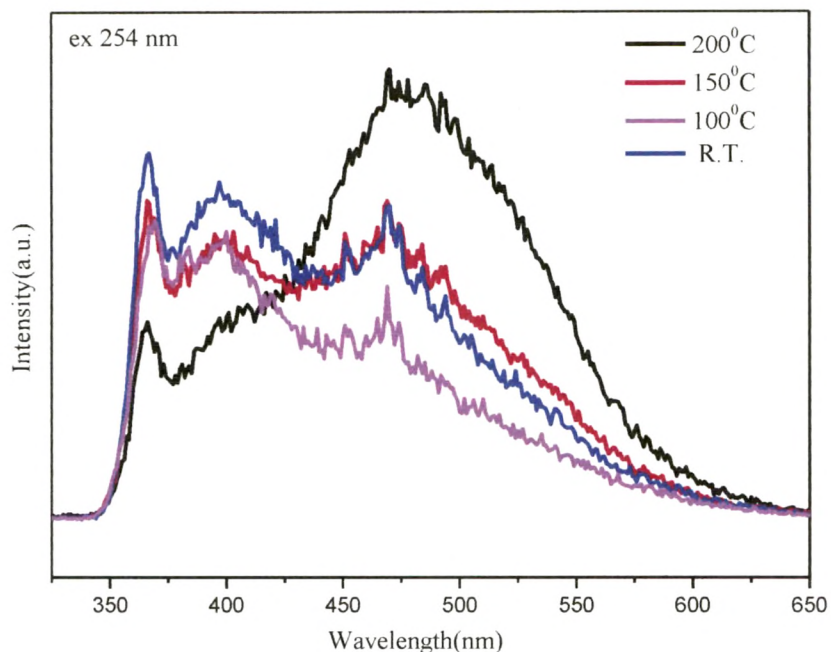


Figure 5.14 PL spectra of $\text{PbWO}_4:\text{Ce}$ prepared at different temperatures excited with 254nm

Figure 5.14 shows room temperature photoluminescence spectra of nanocrystalline $\text{PbWO}_4:\text{Ce}$ powders prepared at different temperatures excited with 254 nm wavelength. PbWO_4 shows broad luminescent emissions in blue and green range. In order to further obtain the detailed parameters about the luminescence properties of PbWO_4 microcrystals, we had fitted the emission spectra using four individual Gaussian lines to achieve good agreement with the experimental data which are shown below Figures 5.14 (a-d). Variation in the location of Gaussian peaks and in their intensity is shown in Table 5.7.

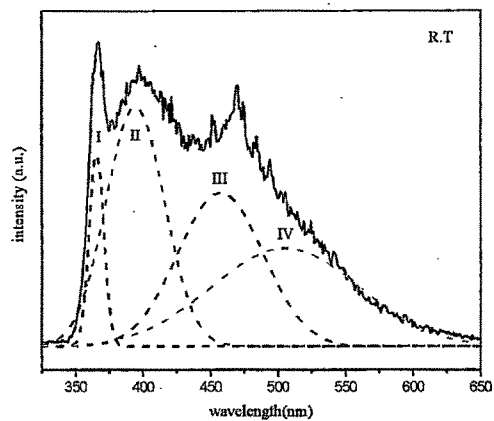


Figure 5.14(a)

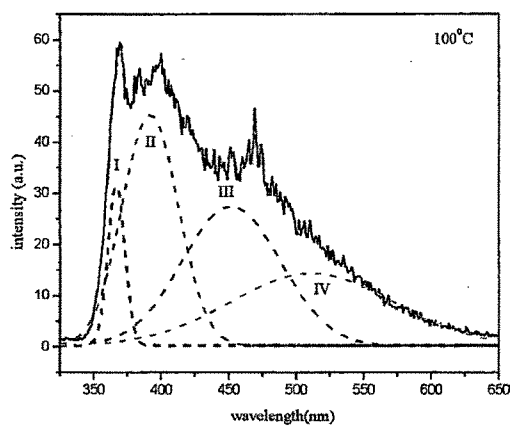


Figure 5.14(b)

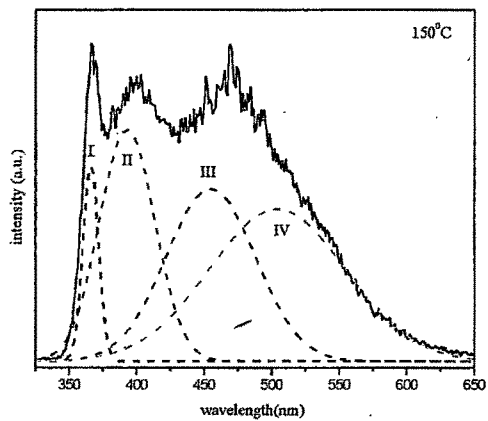


Figure 5.14(c)

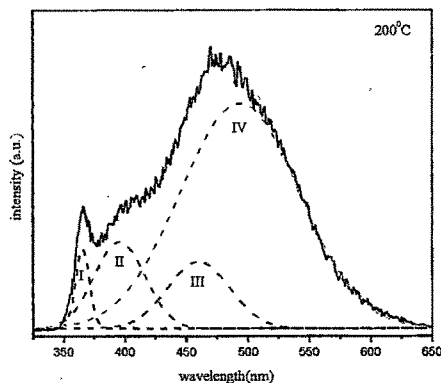


Table 5.7 The locations and intensity of Gaussian components of PL spectra of $\text{PbWO}_4 : \text{Ce}$ samples prepared at different temperatures.

Temp. (°C)	Gaussian peak I		Gaussian peak II		Gaussian peak III		Gaussian peak IV	
	Wavelength (nm)	Intensity (a.u.)	Wavelength (nm)	Intensity (a.u.)	Wavelength (nm)	Intensity (a.u.)	Wavelength (nm)	Intensity (a.u.)
R.T	366	46	394	57	457	37	505	24
100	367	32	392	45	452	27	512	14
150	366	40	393	47	455	35	504	31
200	365	27	396	29	460	23	494	71

As already mentioned earlier the Gaussian peak I is observed at 366 nm, the Gaussian peak II at 397 nm and the Gaussian peak III at 461 nm may correspond to the radiative transitions from ${}^3A_1 \rightarrow {}^1A_1$, ${}^3A_2 \cong {}^3E \rightarrow {}^1A_1$ and ${}^3A_2 \rightarrow {}^1A_1$, respectively from the lower lying triplet state split by Jahn-Teller interaction in the regular WO_4^{2-} complex. The Gaussian peak IV corresponds to oxygen deficient WO_3 irregular complex in scheelite phase.

As we can see from the Table 5.7 positions of B(I) remain almost constant with temperature. The position of B(II) and B(III) components shift to lower energy side and the position of G(IV) component shift towards higher energy side. Intensity of blue components B(I), B(II) and B(III) is higher at low temperatures and low at higher temperature. The

reason for enhancement of green emission for PbWO_4 sample prepared at 200°C is already discussed in the respective section.

5.16 Up Conversion emission (anti-Stokes emission) in PbWO_4

Phosphors that are capable of absorbing photons of a certain energy E_1 and emitting photons with another energy E_2 , such that $E_2 > E_1$. Thus it is also possible to obtain luminescence at photon energies higher than the absorbed photon energy. This is called *anti-Stokes* or *up-conversion luminescence* and it occurs for multilevel systems. As PbWO_4 contains various types of luminescent centers at different energy levels, it is possible to obtain up-conversion luminescence in our system.

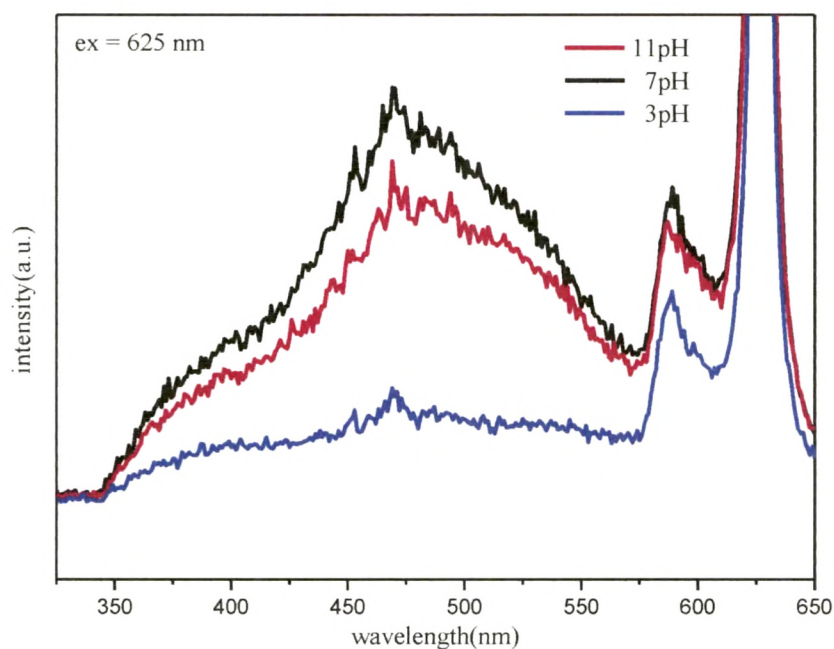


Figure 5.15 Up-conversion luminescence in PbWO_4 synthesized at different pH

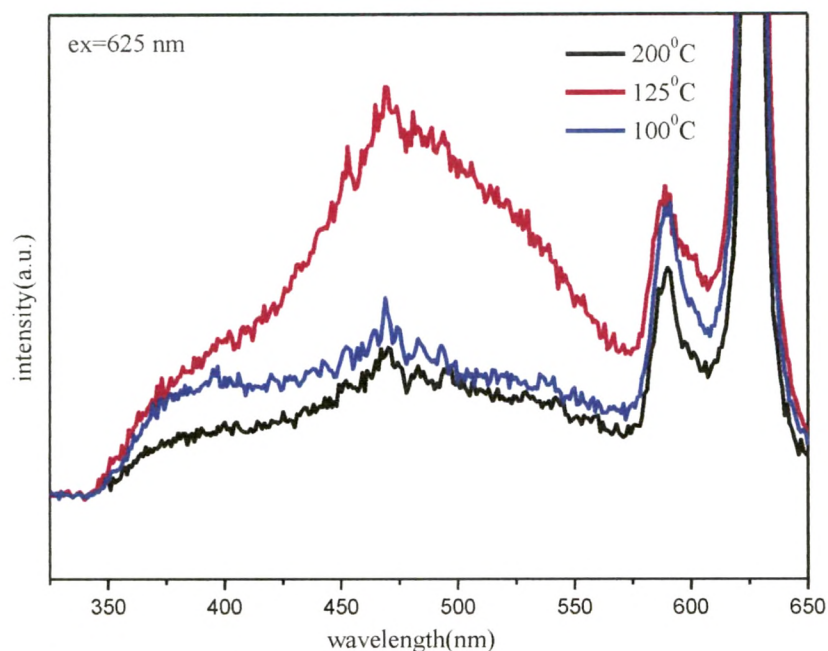


Figure 5.16 Up-conversion luminescence in PbWO_4 synthesized at different temperature

Figure 5.15 and Figure 5.16 shows the up-conversion emission of undoped PbWO_4 synthesized with different pH and temperatures excited with 625 nm wavelength, respectively. In both cases, the same profile of complex emission was observed; and broad blue-green up-conversion emission bands were in the 450–550 nm region (${}^3\text{A}_1 \rightarrow {}^1\text{A}_1$, ${}^3\text{A}_2 \cong {}^3\text{E} \rightarrow {}^1\text{A}_1$, ${}^3\text{A}_2 \rightarrow {}^1\text{A}_1$ and oxygen deficient WO_3 complex) and in the 600 nm region (corresponding to the color center). As shown in both Figures, the intensity of up-conversion luminescence is highest for PbWO_4 sample prepared at 7pH or 125°C, intermediate for 11pH and lowest for 3pH. Up-conversion luminescence intensity is also least for sample prepared at 100°C and 200°C.

5.16.1 Red emission center

There is another luminescent centre in PbWO_4 crystals associated with the red (600nm) luminescence. In Ref. [50, 51] this luminescence is associated with a centre which is caused by the incorporation of the Pb^{3+} centre in PbWO_4 crystals. The trivalent lead ion is stabilized in PbWO_4 crystals by a Frenkel defect (the oxygen ion is shifted to an inter-site position with simultaneous creation of V_O) [52]. Owing to the structure of the valence band the Pb^{3+} -ion does not create a localized hole-type centre. The Frenkel defect in turn lowers the local symmetry of the created WO_3 tungsten complex towards a C_3 , local symmetry or even lower, thus creating the shift and splitting of the original excited energy terms. Such a distorted tungsten anionic complex is responsible for the red luminescence in PbWO_4 crystals.

References

- [1] M.Nikl, presented at the CCC meeting, May 1995, CERN, W. Van Loo, *Phys. Stat. Sol. a.* 27, 1979, 565, W. Van Loo, *Phys. Stat. Sol. a.* 28, 1979, 227.
- [2] J.A. Groenink and G. Blasse, *J. Sol. Stat. Chem.* 32,1980, 9.
- [3] P. Lecoq, I. Dafinei, E. Auffray, M. Schneegans, V. Korzhik, O.V. Missevitch, V.B. Pavlenko, A.A. Fedorov, A.N. Annenkov, V.L. Kostylev, *Nucl. Instrum. Meth.A* 365, 1995, 291.
- [4] Y. Zhang, N.A.W. Holzwarth, R.T. Williams, *Phys. Rev. B* 57, 1998, 12738–12750.
- [5] M.J. Treadaway, R.C. Powell, *J. Chem. Phys.* 61, 1974, 4003–4011.
- [6] Y. Toyozawa, M. Inoue, *J. Phys. Soc. Jpn.* 21, 1966, 1663.
- [7] M. Nikl, P. Bohacek, E. Mihokove, M. Kobayashi; M. Ishii, Y. Usuki, V. Babin, A. Stolovich, S. Zazubovich, M. Bacci, *J. Lumin.* 87–89, 2000, 1136.
- [8] M. Nikl, *Phys. Status Solidi A* 178, 2000, 595.
- [9] J. A. Groenink and G. Blasse, *Journal of solid state chemistry*, 32, 1980, 9-20.
- [10] P. Lecoq, I. Dafinei, E. Auffray, M. Schneegans, M.V. Korzhik, O.V. Missevitch, V.B. Pavlenko, A.A. Fedorov, A.N. Annenkov, V.L. Kostylev, V.D. Ligun, *Nucl. Instr. and Meth. A* 365,1995, 291.
- [11] M.V. Korzhik, V.B. Pavlenko, T.N. Timoschenko, V.A. Katchanov, A.V. Singovskii, A.N. Annenkov, V.A. Ligun, I.M. Solskii, J.-P. Peigneux, *Phys. Status Solidi A*, 154, 1996, 779.
- [12] A. Annenkov, E. Auffray, M. Korzhik, P. Lecoq, J.-P. Peigneux, *Phys. Status Solidi A*, 1998,170.
- [13] M.V. Korzhik, *Zh. Prikl. Spekt.* 61,1994, 83.
- [14] J.A. Groenink, G. Blasse, *J. Solidi State Chem.* 32, 1980,9.
- [15] M.V. Korzhik, V.B. Pavlenko, T.N. Timoschenko, V.A. Katchanov, A.V. Singovskii,

- A.N. Annenkov, V.A. Ligun, I.M. Solskii, J.-P. Peigneux, *Phys. Status Solidi A* 154, 1996, 779.
- [16] A. Annenkov, E. Auffray, M. Korzhik, P. Lecoq, J.-P. Peigneux, *Phys. Status Solidi A* 170, 1998, 47.
- [17] M.V. Korzhik, V.B. Pavlenko, T.N. Timoschenko, V.A. Katchanov, A.V. Singovskii, A.N. Annenkov, V.A. Ligun, I.M. Solskii, J.-P. Peigneux, *Phys. Status Solidi A* 154, 1996, 779.
- [18] M.V. Korzhik, *Zh. Prikl. Spekt.* 61, 1994, 83.
- [19] M. Itoh, M. Fujita, *Phys. Rev. B* 62, 2000, 12825.
- [20] M. Itoh, D.L. Alov, M. Fujita, *J. Lumin.* 87–89, 2000, 1243.
- [21] D.L. Alov, N.V. Klassen, N.N. Kolesnikov, S.Z. Shmurak, in: P. Dorenbos, C.W.E. van Eijk (Eds.), *Proceedings of the International Conference on Inorganic Scintillators and their Applications*, Delft University Press, The Netherlands, 1996, p. 267.
- [22] D.L. Alov, S.I. Rybchenko, *Mater. Sci. Forum* 239–241, 1997, 279.
- [23] A.A. Annenkov, M.V. Korzhik, P. Lecoq, *Nucl. Instr. and Meth. A* 490, 2002, 30.
- [24] M. Kobayashi, M. Ishii, K. Harada, Y. Usuki, H. Okuno, H. Shimizu, T. Yazawa, *Nucl. Instr. and Meth. A* 373, 1996, 333.
- [25] R.Y. Zhu, D.A. Ma, H.B. Newman, C.L. Woody, J.A. Kierstead, S.P. Stoll, P.W. Levy, *Nucl. Instr. and Meth. A* 376, 1996, 319.
- [26] M. Boehm, A.E. Borisevich, G.Yu. Drobychev, A. Hofstaetter, O.V. Kondratiev, M.V. Korzhik, M. Luh, B.K. Meyer, J.-P. Peigneux, A. Scharmann, *Phys. Status Solidi A* 167, 1998, 243.
- [27] A. Hofstaetter, R. Oeder, A. Scharmann, D. Schwabe, B. Vitt, *Phys. Status Solidi B* 89, 1978, 375.
- [28] J.M. Moreau, R.E. Gladyshevskii, Ph. Galez, J.P. Peigneux, M.V. Korzhik, *J. Alloys*

- Compounds 284, 1999, 104.
- [29] M.V. Korzhik, Delft University Press, Delft The Netherlands, 1996, p. 241.
- [30] C. Shi, Y. Wei, X. Yang, D. Zhou, C. Guo, J. Liao, H. Tang, Chem. Phys. Lett. 328, 2000, 1.
- [31] L. Sun, Q. Guo, X. Wu, S. Luo, W. Pan, K. Huang, J. Lu, L. Ren, M. Cao, C. Hu, J. Phys. Chem. C 111, 2007, 532
- [32] D.Tawde, M.Srinivas & K.V.R.Murthy, physics status solidi a, Vol.208, Issue 4, 2011, 803- 807.
- [33] A. Changhua, T. Kaibin, S. Guozhen, W. Chunrui, and Q. Yitai, Mater. Lett. 57, 2002, 565.
- [34] W.Van Loo, Phys. Status Solidi A 27, 1975, 565.
- [35] Biao Liu, Shu-Hong Yu, Linjie Li, Qiao Zhang, Fen Zhang, and Ke Jiang, Angew. Chem., 116, 2004, 4849-4854.
- [36] M. Nikl, V. V. Laguta, and A. Vedda, Phys. Status Solidi B 245, 2008, 1701.
- [37] A. Annenkov, E. Auffray, M. Korzhik, P. Lecoq, and J.-P. Peigneux, Phys. Status Solidi A 170, 47 (1998).
- [38] M. Itoh, D. L. Alov, and M. Fujita, J. Lumin., 87, 2000, 1243.
- [39] Changhua An, Materials Letters 57, 2002, 565- 568.
- [40] M. Nikl, P. Bohacek, E. Mihokove, M. Kobayashi, M. Ishii, Y. Usuki, V. Babin, A. Stolovich, S. Zazubovich, M. Bacci, J. Lumin. 87-89 , 2000, 1136.
- [41] Y. Zhang, N. A. W. Holzwarth, and R. T. Williams, Phys. Rev. B 57, 1998, 12738.
- [42] M. Bacci, S. Porcinai, E. Mihóková, M. Nikl, and K. Polák, Phys. Rev. B 64, 2001, 104302.
- [43] Y. Zhang, N. A. W. Holzwarth, and R. T. Williams, Phys. Rev. B 57, 1998, 12738.
- [44] G. Blasse, Struct. Bonding ,Berlin, 42, 1980, 1.

- [45] M. Itoh and T. Sakurai, *Physical Review B* 73, 2006, 235106.
- [46] M. J. J. Lammers, G. Blasse, and D. S. Robertson, *Phys. Status Solidi A* 63, 1981, 569.
- [47] V. B. Mikhailik, H. Kraus, D. Wahl, M. Itoh, M. Koike, and I. K. Bailiff, *Phys. Rev. B* 69, 2004, 205110.
- [48] Yanlin Huang, Xiqi Feng, Wenliang Zhu, Zhenyong Man, *Journal of Crystal Growth* 250, 2003, 431–436.
- [49] Belsky, A. N.; Mikhailin, V. V.; Vasil'ev, A. N.; Dafinei, I.; Lecoq, P.; Pedrini, C.; Chevallier, P.; Dhez, P.; Martin, P. *Chem. Phys. Lett.* 243, 1995, 552.
- [50] P. Lecoq, I. Dafinei, E. Auffray, M. Sneegans, M.V. Korzhik, O.V. Missevitch, V.B. Pavlenko, A.A. Fedorov, A.A. Annenkov, V.L. Kostilev, V.D. Liogun, *Nucl. Instr. and Meth. A* 365 (1995) 291.
- [51] A.A. Annenkov, A.A. Fedorov, Ph. Galez, V.A. Kachanov, M.V. Korzhik, V.B. Pavlenko, V.A. Ligun, T.N. Timochenko, J.-P. Peigneux, B.A. Zadneprovski, *Phys. Stat. Sol. A* 156 (1996) 493.
- [52] A. Fedorov, M. Korzhik, O. Missevitch, et al., *Radiat. Meas.* 26, 1996, 107.